1 λ, 6 bits/symbol, 280 and 350 Gb/s Direct Detection Transceiver using Intensity Modulation, Polarization Multiplexing, and Inter-Polarization Phase Modulation

[†]M. Chagnon, M. Osman, D. Patel, V. Veerasubramanian, A. Samani, and D.V. Plant
McGill University, Photonic Systems Group, 3480 University St., Montreal, Canada, H3A 0E9
[†]mathieu.chagnon@mail.mcgill.ca

Abstract: We demonstrate 1λ, 6 bits/symbol, 280 and 350 Gb/s throughput with direct detection of polarization multiplexed PAM-4 intensity modulation and inter-polarization phase modulation over 4 phases at BERs of 2.5×10−3 (<HD-FEC) and 1.6×10−2 (<SD-FEC), respectively.
OCIS codes: (060.2330) Fiber optics communications; (060.4080) Modulation

1. Introduction

Driven by the unabated growth of data center hosted cloud applications and services, the demand for faster short reach optics is growing incessantly. Externally modulating a single laser to produce 100 Gb/s capacities is desirable as it provides a more scalable solution than a multiplexing approach for next generation 400 Gb/s and 1Tb/s targets. Recent 100 Gb/s short-reach IM/DD transmission experiments have been reported using various advanced modulation formats, such as PAM-4 with PDM [1], half-cycle Nyquist subcarrier PDM 16-QAM [2], multi-band CAP [3], and DMT [4]. PDM was also used in a self-coherent system experiment in [5]. We recently reported in [6] 112 Gb/s PAM transmission, and extended this work to include PDM for 224 Gb/s over 10 km [7].

In this paper, we report a 280 Gb/s and 350 Gb/s transceiver using a single 1550 nm laser which is intensity modulated (IM) over 4-levels on 2-polarizations with 4-phase inter-polarization phase modulation (PM) and using direct detection (DD) at a spectral efficiency of 6 bits/symbol. Bit error rates (BER) are below the hard-decision and soft-decision FEC thresholds of 3.8×10^{-3} and 2×10^{-2}, allowing data throughput of 250 and 280 Gb/s with 12% and 25% protocol/FEC overhead, respectively. The DP−PAM-4+4PM format is demultiplexed at the receiver using a novel DSP that operates in a 4 dimensional (4D) power space after DD. To the best of our knowledge, this is the first demonstration of DD reception of a 280 and 350 Gb/s signal.

2. Principle of self-beat direct detection of polarization multiplexed IM with PM

A block diagram of the polarization division multiplexed intensity and phase modulation / direct-detection (PDM IPM/DD) system is shown in Fig. 1. The transmitter in Fig. 1 a) externally intensity modulates a single laser on two orthogonal states of polarization (SOPs). One IM is followed by a phase modulator which modulates the phase difference between the two orthogonal SOPs before being polarization combined, allowing modulation over three degrees of freedom. Fig. 1 b) shows the receiver front-end as reported in our previous work [7]. The four detected signals are fed into the DSP stack of Fig. 1 c) which achieves polarization demultiplexing and signal detection of the two orthogonal IM signals and of the inter-polarization phase modulation signal. The first stage of the DSP stack is a 4×4 MIMO that inverts the polarization rotation and mitigates mainly receiver-side inter-symbol interference (ISI). Four error signals are evaluated as the difference between the desired equalizer outputs and the four current outputs. The error signals are used to update the taps of all 16 FIR filters of the 4×4 MIMO using their respective inputs, updated using the stochastic gradient descent algorithm. More specifically, the equalizer is initially updated using training symbols before switching to a decision-directed mode. The second stage in Fig. 1 c) comprises four SISO FIR filters that are used to remove any residual ISI uncompensated by the first stage, and mainly residual transmitter-side ISI. Finally, estimates of the three information streams are obtained.

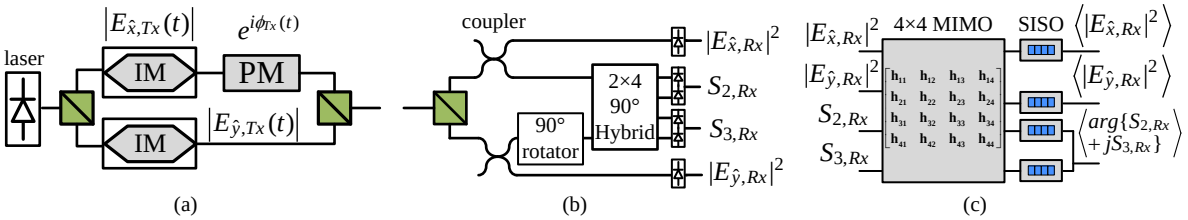

Fig. 1. Block diagram of PDM IPM/DD system showing a) transmitter b) receiver front-ends, and c) 2-stage MIMO/SISO DSP stack

The transmitted and received fields can be represented by 4D power vectors in the form $[|E_{\hat{x}}|^2, |E_{\hat{y}}|^2, S_2, S_3]^{\mathrm{T}}$, where $S_2 = 2Re\{E_{\hat{x}}E_{\hat{y}}^*\}$ and $S_3 = -2Im\{E_{\hat{x}}E_{\hat{y}}^*\}$. SOP rotation in SMF can be represented by a unitary rotation matrix that is applied to the transmitted Jones vector $[E_{\hat{x},Tx}, E_{\hat{y},Tx}]^{\mathrm{T}}$. Using a generic matrix of elements *a* and *b* with relation $|a|^2+|b|^2=1$, Eq. (1) shows the 4-by-4 matrix relating the received and transmitted 4D power vectors.

$$\begin{bmatrix} E_{\hat{x},Rx} \\ E_{\hat{y},Rx} \end{bmatrix} = \begin{bmatrix} a & -b \\ b^* & a^* \end{bmatrix} \begin{bmatrix} E_{\hat{x},Tx} \\ E_{\hat{y},Tx} \end{bmatrix} \Rightarrow \begin{bmatrix} |E_{\hat{x},Rx}|^2 \\ |E_{\hat{y},Rx}|^2 \\ S_{2,Rx} \\ S_{3,Rx} \end{bmatrix} = \begin{bmatrix} |a|^2 & |b|^2 & -Re\{ab^*\} & -Im\{ab^*\} \\ |b|^2 & |a|^2 & Re\{ab^*\} & Im\{ab^*\} \\ 2Re\{ab\} & -2Re\{ab\} & Re\{a^2\}-Re\{b^2\} & Im\{a^2\}+Im\{b^2\} \\ -2Im\{ab\} & 2Im\{ab\} & Im\{b^2\}-Im\{a^2\} & Re\{a^2\}+Re\{b^2\} \end{bmatrix} \begin{bmatrix} |E_{\hat{x},Tx}|^2 \\ |E_{\hat{y},Tx}|^2 \\ S_{2,Tx} \\ S_{3,Tx} \end{bmatrix} \quad (1)$$

In Fig. 1 a), the Jones vector is $[|E_{\hat{x},Tx}(t)|, |E_{\hat{y},Tx}(t)|e^{j\phi_{Tx}(t)}]^{\mathrm{T}}$ with powers $|E_{(\hat{x},\hat{y}),Tx}(t)|^2$ per polarization, one of which receiving a 4-level PM signal. The last 2 elements of the derotated vector provides phase data via $\angle(S_2+jS_3)$.

3. Experimental setup

A schematic of the experimental setup is shown in Fig. 2. At the transmitter, a 14.3 dBm laser diode (LD) at 1550 nm is intensity modulated by a 41 GHz silicon photonic modulator [8], driven by an amplified 70 GSamples/s 8-bit digital to analog converter (DAC) channel. The single polarization IM light at −4 dBm is amplified by an EDFA and filtered by a 0.8 nm tunable filter to remove out-of-band noise. A polarization controller (PC) aligns the SOP to the axis of a polarization maintaining splitter before entering the dual polarization emulator. One output port is phase modulated by a low-Vπ LiNbO3 PM that is driven by another DAC channel and allows modulating a phase difference between the two orthogonal IM signals. The other output port is delayed by a variable optical delay line ($VODL_2$) allowing recombination at the polarization beam combiner (PBC) with the desired optical path difference. An optical on-off switch and two PCs allow for comparing and equating the power on each polarization after the PBC. Before the emulator, $VODL_1$ delays the IM waveform such that the PM waveform is applied at the proper time on the IM field. We note that several components used in the Fig. 2 transmitter (e.g. EDFA, filter, PCs) for the experimental demonstration would not be required when realizing the fully integrated transmitter shown in Fig. 1 a).

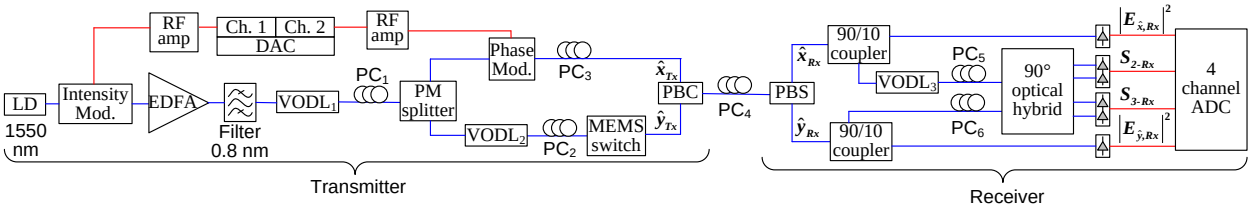

Fig. 2. Experimental setup (blue lines = optical; red lines = electrical)

The receiver in Fig. 2 is composed of a polarization beam splitter (PBS) that separates the received signal on two fixed orthogonal polarization axes, followed by two 90/10 couplers. The 10% ports of each coupler go to two PIN+TIA photoreceivers, generating $|E_{\hat{x},Rx}|^2$ and $|E_{\hat{y},Rx}|^2$. Uneven coupling ratios were necessary as the 2 balanced photodetectors (BPDs) following the hybrid did not have TIAs. Optical time alignment is assured prior to entering the hybrid. The 2 BPDs generate the receiver's $S_{2,Rx}$ and $S_{3,Rx}$. A 4 channel, 8-bit 80 Gsamples/s analog to digital converter (ADC) real-time samples the 4 received waveforms for offline processing. The transmitter DSP for generating the IM is that reported in our previous work [6]. Similar processing applies to the PM signal, without the MZM arcsin compensation. At the receiver, the 4 waveforms are first resampled at 2 samples per symbol before being fed to the 2-stage DSP stack of Fig. 1 c). Finally, hard decision is performed and the BER is calculated.

4. Results

BER performance over varying bit rates and SOPs are presented. In Fig. 3 a), we vary the symbol rate of the 6 bits/symbol DP−PAM4+4PM format from 28 Gbaud to 58.4 Gbaud and recover information using the DSP presented above. BERs below the HD-FEC threshold are obtained up to ≈300 Gb/s, while a BER of 1.6×10^{-2} is obtained at a throughput of 350 Gb/s, below the SD-FEC threshold. Crosses at 280 Gb/s and 350 Gb/s are added as those bitrates represent 250 Gb/s and 280 Gb/s of data payload below HD and SD-FEC with respective overheads of 12% and 25%. Fig. 3 b) shows the performance degradation on the intensity modulation when phase modulation is enabled, for both single polarization (SP) and dual polarization (DP), using the MEMS on-off switch. As we are generating all possible transmission configurations, namely SP or DP with PM on or off, the DSP stack presented

for the full DP−PAM4+4PM format cannot be applied. In order to de-embed the SOP rotation penalty form the application of PM in this study, we align the SOP to the receiver's axes and use regular PAM4 IM/DD DSP, as we reported in [6], on available IM signals present on the receiver. Fig. 3 b) shows the strong deterioration of the intensity modulated signals, on both orthogonal polarizations, even if PM is applied to only one polarization axis. At 42 Gbaud, turning the PM on increases the BER 50-fold, while at 56 Gbaud it increases from $\approx 10^{-3}$ to 8×10^{-3}. The deterioration of the IM signal due to PM is because of the undesired amplitude modulation components that arise from generating the optical phase modulated signal [9]. The larger deterioration at lower symbol rates is due to the larger available RF swing on the PM with decreasing symbol rates. Finally, Fig. 3 c) presents the BER of the DP−PAM4+4PM format at 56 Gbaud as the received SOP is varied from 0° to 45° and processed with the MIMO/SISO receiver DSP. The rising BER with increasing rotation angle $\theta=arcsin(|b|)$ from 0° to 45° occurs because the received signal power on the two PIN+TIAs increases as the cross term $2Re\{ab^*\}$ in $|aE_{\hat{x},Tx} - bE_{\hat{y},Tx}|^2$ grows. If the received power is optimized at 0°, the TIAs will begin to saturate with increasing angle to the point where the received power is almost doubled when the angle reaches 45°. Moreover, each of the four photoreceivers/detectors has its own frequency response that induces ISI on the received power vectors. As the angle increases, there will be an increased penalty associated with using a small number of taps in the first derotation stage, as the second stage SISOs are not able to cancel residual cross talk from other channels. Finally, Fig. 4 shows the eye diagrams of the IM PAM4 on $\hat{x}$ and $\hat{y}$ and the 4 phases of the PM at 28 and 56 Gbaud, as found in Fig. 3a).

We note here that at 1550 nm, the demonstration wavelength, propagation of signals with this modulation format over short distances was not feasible because of the inherent interplay between phase modulation and chromatic dispersion (CD). It is known that chromatic dispersion converts phase modulation to intensity modulation [10]. This CD–PM interplay would be strongly minimized by operating around 1310 nm which, as per IEEE Std 802.3ba, is the defined operating wavelength for short reach optics.

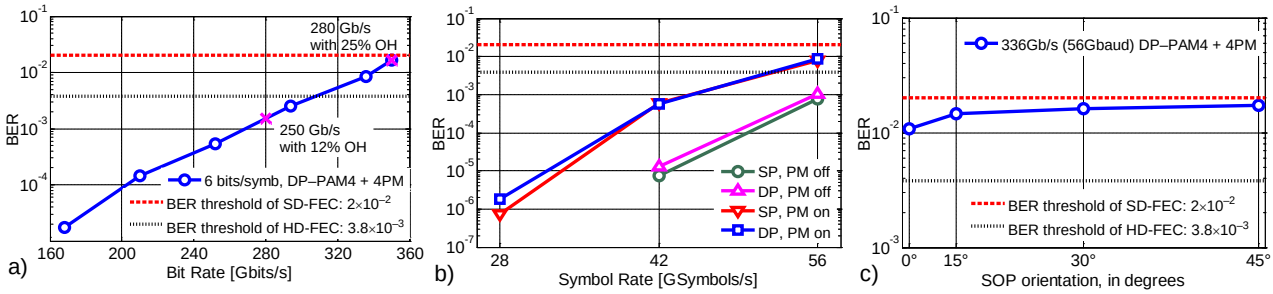

Fig. 3. a) BER vs bit rate for DP−PAM4+4PM, b) BER degradation of IM when enabling PM, c) 56 Gbaud DP−PAM4+4PM over varying SOP

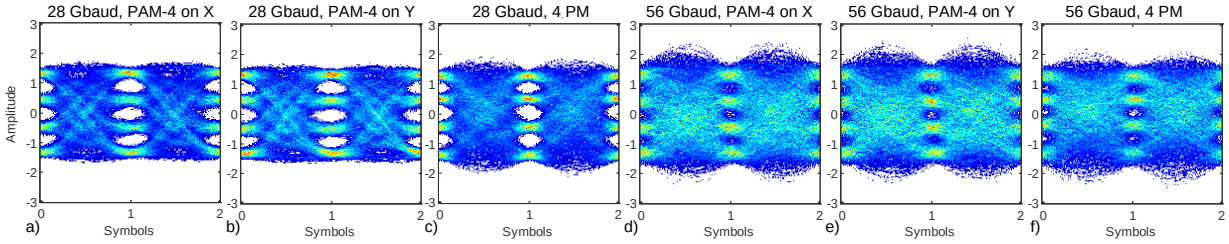

Fig. 4. Eyes diagrams of recovered IM on each polarization and recovered inter-polarization PM, at a) – c) 28 Gbaud and d) – f) 56 Gbaud

5. Conclusion

A polarization multiplexed intensity with inter-polarization phase modulation transceiver using direct-detection is demonstrated at 280 and 350 Gb/s below the HD and SD-FEC thresholds on a single wavelength. A novel two-stage 4-by-4 MIMO / SISO receiver DSP operating on the 4D power space after a direct detection receiver is presented and employed for derotation and symbol recovery. All components of the transmitter and receiver can be fabricated and integrated on a single chip operating at 1310 nm using demonstrated silicon photonics components.

5. References

[1] R. Rodes, *et al.*, OFC, paper PDP5D.10, 2012
[2] A. Karar, *et al.*, ECOC, paper PDP Th.3.A.4, 2012
[3] M. I. Olmedo, *et al.*, J. Lightwave Technol., vol. 32, no. 4, 2014.
[4] W. Yan, *et al.*, OFC, paper OM3H.1, 2013
[5] D. Che, *et al.*, Opt. Lett., vol. 39, no. 11, 2014
[6] M. Chagnon, *et al.*, Opt. Exp. vol. 22, no.17, 2014
[7] M. Morsy-Osman, *et al.*, ECOC, paper PD.4.4, 2014
[8] D. Patel, *et al.*, CLEO, paper SW3N.3, 2015.
[9] S. Norimatsu, *et al.*, J. Lightwave Technol., vol. 11, no. 5, 1993
[10] J. Wang, *et at.*, J. Lightwave Technol., vol. 10, n. 1, 1992